Dusty Plasma in the Earth and in Space: Experiments

V. E. Fortov, O. F. Petrov, O. S. Vaulina

Institute for High Energy Densities, RAS, Moscow, Russia

Abstract. Results of a complex experimental study of the transport properties of dusty plasmas (the diffusion, viscosity, and thermal conductivity constants; the ambipolar diffusion of dust charging by the photo-emissive mechanism; the self-diffusion of dust particles in plasma) are presented. The experiments were performed for a wide range of dusty plasma parameters under the ground-based, and microgravity conditions.
PACS: 52.27.Lw, 52.27.Gr, 52.35.Fp

1. INTRODUCTION

The problems associated with the transport phenomena in systems of interacting particles are of significant interest in various fields of science and technology (plasma physics, medical industry, physics of polymers, etc.) [1-9]. The main problem in studies of such systems is associated with the absence of an analytical theory of liquid that could explain its thermodynamic properties, describe heat and mass transfer and so on. At present, the theory of strongly coupled systems is developing using two basic approaches. One of them consists in numerical calculation of properties of a medium using model data on the particle interaction [9-18]; the second method is based on analogies between the crystalline and liquid states of matter [2,4].

The dusty plasma (consisting of electrons, ions, neutral gas and macroparticles of micron sizes) is ubiquitous in nature and often appears in a number of technological processes. Laboratory dusty plasma is a good experimental model for studying of non-ideal systems and for proofing existing empirical models and numerical results, because, owing to their size, dust particles may be videofilmed, which significantly simplifies the use of direct diagnostic methods [17-34]; this enables one to investigate the transport processes on the kinetic level. The most experiments on the study of physical properties of this plasma are performed in the gas discharges, where macroparticles can acquire a considerable negative charge ($\sim 10^3$-10^5e) and may interact electrostatically with one another. The main source of the kinetic energy dissipation for macroparticles in weakly ionized plasma is their collisions with neutrals of a buffer gas. The joint action of the interparticle interaction and dissipative processes may lead to the formation of steady-state dust structures (as a liquid or a solid) as well as to complex vibrational or stochastic modes.

Under standard laboratory conditions, the observed dust structures are confined in the Earth gravity field by the electric field of the strata (in a dc- discharge) or by the electrode layer (in an rf- discharge), while the gravity field sets a limit on the experimental results. In recent years, considerable attention is paid to experimental studied of dusty plasmas under microgravity conditions [19-21, 30-33]. Such experiments make it possible to study a wide range of phenomena (photo-emissive charging of atmospheric aerosols, dynamics of massive dust particles, and so on), which cannot be observed in ground-based laboratory conditions. One of important advantages of experiments in microgravity is the possibility to operate in a wide range of dusty plasma parameters, which is not limited by the necessity to ensure levitation of particles in the gravity field.

In this paper, the results of a complex study of transport properties of dusty plasmas are presented for the ground-based, and microgravity conditions. In Section 2 the analytical relations between the basic transport constants (diffusion, viscosity, thermal conductivity and thermal diffusivity) are considered for simple fluids. Section 3 deals with the experimental study of these transport constants for the dust in plasmas in ground-based conditions. Section 4 deals with the results and analysis of experiments on the study of the transport properties of dusty plasma (the ambipolar diffusion of dust charging by the photo-emissive mechanism; the diffusion) that were carried out in the microgravity conditions.

2. RELATIONS BETWEEN TRANSPORT CONSTANTS

The coefficients of diffusion D, thermal conductivity χ, and viscosity η are fundamental parameters that reflect the nature of the interparticle potentials and the phase state of the systems. In the case of gases, the constants of diffusion D, kinematical viscosity $\nu = \eta/\rho$, and thermal diffusivity $\theta = \chi/(\rho\, c_p)$ are close in value and may be written in the form of known analytical relations (here $\rho = M\, n$, where M and n are the particle mass and concentration, and c_p is the specific heat capacity at constant pressure). The numerical simulation of transport processes in simple monatomic dense liquids with a wide scope of interaction potentials reveals that [4]

$$\eta \cong T/(8.1\, l_p D), \tag{1}$$

$$\theta \cong \frac{0.75 k_B}{M c_p} l_p V_t \left(\frac{0.6 l_p V_t}{D} \right)^{5/8}, \tag{2}$$

where $c_p = 2.5\, k_B/M$, $V_T = (T/M)^{1/2}$, and l_p is the mean interparticle distance,

There are at least two essential differences between the molecular fluids and the dissipative systems such as dusty plasmas or the various biological and chemical systems. These are the different potential of interparticle interaction and the presence of an external friction due to the collisions of macroparticles with the atoms/molecules of the surrounding medium. It is customary to assume that dust particles in plasma interact with one another through the screened Coulomb potential, $\phi = (eZ)^2 \exp(-l/\lambda)/l$, where λ is the screening radius, and eZ is the dust charge. A study of the transport constants for the dust systems in plasmas is of great interest [7-18, 24-26]. The various scaling laws for the temperature dependencies of these constants were proposed for two- (2d-), and three- (3d-) dimensional systems with this potential in the works [10-18]. A comparison of these numerical results shows that two parameters, Γ^* and $\xi = \omega^*/\nu_{fr}$, are responsible for the transport processes in these systems with $\kappa = l_p/\lambda < 6$, and $20 < \Gamma^* < 110$ [10,16]; here $\Gamma^* = a_1\, \Gamma\, (1+\kappa+\kappa^2/2) \exp(-\kappa)$, $\omega^* = eZ\, [a_2(1+\kappa+\kappa^2/2) \exp(-\kappa)/(\pi M l_p^3)]^{1/2}$, $\Gamma = (eZ)^2/(T\, l_p)$, ν_{fr} is the friction coefficient, and $a_2 \equiv 1$ for 3d- problem; $a_2 = 2$ for the 2d- case.

In the case of weakly dissipative systems ($\nu_{fr} << \omega^*$, $\xi \to \infty$), the results of simulation of the dynamics for macroparticles in plasma and simple liquids coincide. In order to include the effects of dissipation, the scaling parameter ξ must be taking into account [10, 16]. The normalized transport constants, $D^*(\Gamma^*) = D(1+\xi)/(\omega^* l_p^2)$ and $\nu^*(\Gamma^*) = \nu/[(\omega^* l_p^2)\,(1+\xi)]$ are shown in Fig. 1, where the normalized thermal diffusivity $\theta^* = \theta/[(\omega^* l_p^2)\,(1+\xi)^{5/8}]$ (retrieved from Eq. 2, and the diffusion simulations) is also shown. Notice, that for $\xi \to \infty$: $D^* \to D/(\omega^* l_p^2)$; $\nu^* \to \nu/(\omega^* l_p^2)$; $\theta^* \to \theta/(\omega^* l_p^2)$.

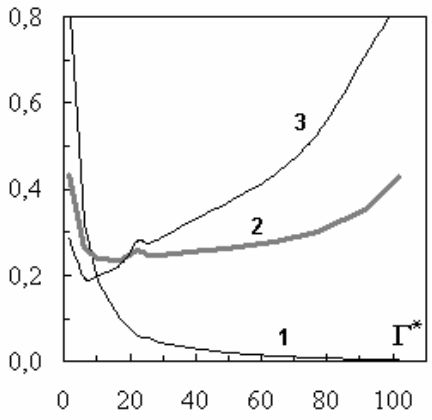

FIGURE 1. Normalized transport constants D^* (**1**), θ^* (**2**) и ν^* (**3**) vs. Γ^* for the systems with the screened Coulomb potential.

3. STUDY OF TRANSPORT PROPERTIES OF DUSTY PLASMA UNDER GROUND-BASED CONDITIONS

3.1. Experimental study of viscosity and diffusion for macroparticles in dusty plasma

To determine the relationship between the viscosity and diffusion constants for dense fluids, the Einstein-Stokes (E-S) relation is commonly used [3, 4, 16-18]: $\nu \propto T/D$ (see Eq. (1)). The experiments in the molecular fluids lend support to the validity of

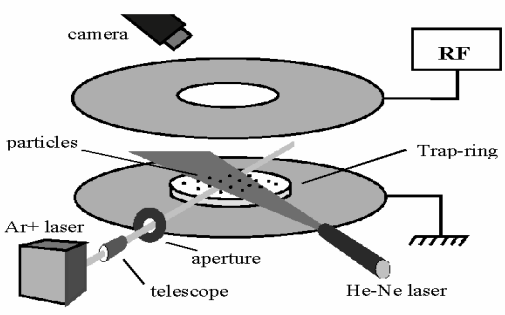

FIGURE 2. Schematic of the experimental setup.

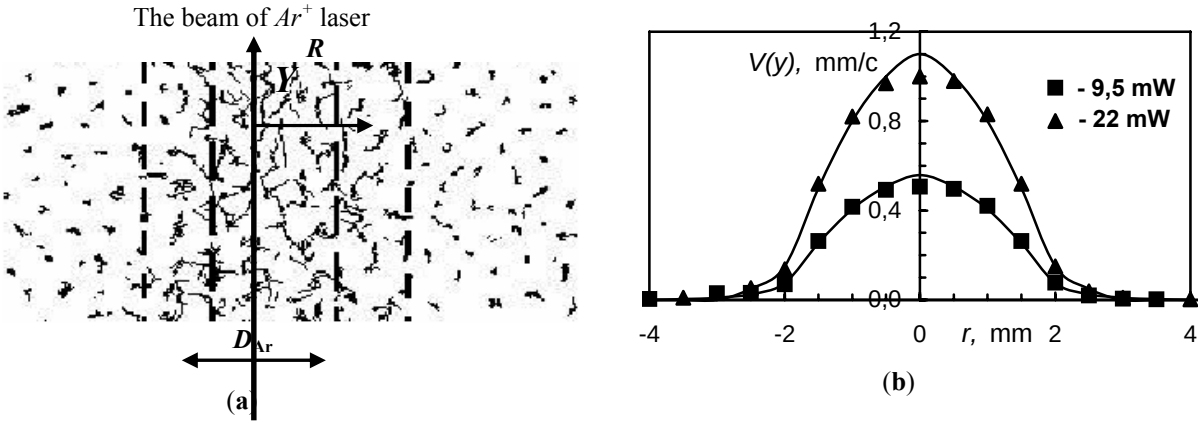

FIGURE 3. Illustration of trajectories for dust particles (a) and (b) - the measured velocities $V(y)$ (figures) for two different powers of Ar^+ laser radiation W together with their approximation by the Navier-Stokes equation (hard lines).

E-S relation over a wide range of temperature. Here we present the results of the first experimental examination of this relation for macroparticles in dusty plasma. The experimental study of the diffusion and viscosity for dust systems was performed in RF- discharge in argon at pressure $P \sim 10$ -100 Pa with discharge power $W_d \sim 2$ - 20 W. The dust component was provided by particles of formaldehyde melamine of density $\rho_p \approx 1.5$ g cm^{-3} and different radius $a_p \approx$ 0.95 μm; 1.7 μm; 6.73 μm. The scheme of experiment is shown in Fig. 2. The observed dust clouds were the liquid structures consisting of ~15 dust layers. The radiation of Ar^+ laser was used for a formation of laminar flow of particles moved through an undisturbed area of dust cloud. The beam of Ar^+ laser was pre-expanded by a telescope, and the central part of this beam was cut out by a diaphragm of diameter $D_{Ar} \cong 3$ mm. The power of Ar^+ laser radiation W was ~5 -200 mW. For diagnostics, a plane beam of *He-Ne* laser (~ 250 μm) illuminated the dust layer, which was videofilmed using a high-speed CMOS camera (frequency 500 s^{-1}).

As a suitable approximation for the viscosity determination we have solved the Navier-Stokes equation in the cylindrical symmetry: $\nu M \frac{1}{r}\frac{\partial}{\partial r} r \frac{\partial V(y)}{\partial r} = -F(r) + \nu_{fr} M V(y)$, where $F(r)$ is the laser radiation force. The viscosity constants, ν, were obtained by the best fitting of velocity profiles $V_y = V(y)$ (see Fig. 3). The similar techniques were applied in [7, 8]. The measured values of ν, T and l_p are presented in Table 1 for the low radiation of Ar^+ laser (W < 30 mW). In this case, the parameters (T and l_p) measured in dust flow were in agreement with those in the undisturbed plasma, and $T_r \cong T_y$. As the dust parameters in the dust flow in the case of low laser radiation are close to ones in undisturbed systems, we may compare the obtained viscosity coefficients with the diffusion constants measured in undisturbed dust area.

TABLE 1. Mean interparticle distance (l_p) , temperature (T), diffusion (D) and viscosity (ν) coefficients, coupling parameter (Γ^*), and scaling factor (ξ) for different particle sizes (a_p), discharge power (W_d) and gas pressure (P).

P/W$_d$ *(Pa) /(mW)*	**a_p (μm)**	**l_p (μm)**	**T (eV)**	**D x10^5 (cm^{2}s^{-1})**	**ν (cm^{2}s^{-1})**	***C***	***Γ**** **2d/3d**	**ξ 2d/3d**
15/7	0.95	780	0.026	1.54	0.40	8.75	98/87	0.109/0.089
25/13	0.95	600	0.035	1.98	0.25	7.74	69/62	0.083/0.068
98/15	1.7	800	0.3	1.16	1.12	8.76	87/78	0.042/0.034
67/20	1.7	670	0.42	1.16	3.33	7.62	58/52	0.069/0.057
19/15	6.37	720	40.6	50.9	0.052	7.82	44/42	0.73/0.59
19/5	6.37	800	27.4	22.6	0.094	8.15	80/73	0.73/0.59
11/2	6.37	890	48.7	27.7	0.163	8.43	106/95	2.32/1.90

In diffusion measurements the ratio of mean square displacement, $<\Delta l^2>=<\Delta y^2>+<\Delta r^2>$, to the observation time t is usually calculated. The diffusion constant, $D = \lim_{t\to\infty} D(t)$, in our case can be obtained from the relation: $D(t) = <<\Delta l^2>_N>_t/4t$, where Δl is the displacement of a dust particle for the time t, and the brackets $< >$ denote the ensemble (N), and time (t) average. The illustration of measured $D(t)$- functions is shown in Fig. 4. The measurements were performed for t_{exp}~ 8-10 s ($\omega^* t_{exp} \sim 100$); in doing so the $D(t)$ values were equal to the D constant, within the experimental errors, at $t > 3.5$-5 s (at $\omega^* t > 50$). The results of measurements (D, ν, T and l_p) are presented in Table 1. Experimental error was less than 5% for T and D, less than 10% for ν, and less than 3% for l_p.

For dense fluids, the E-S relation between the shear viscosity $\eta = Mn\nu$ and diffusion constants D is commonly used: $\eta \cong T/(6\pi D a_{eff})$; here $n = l_p^{-3}$ is the concentration, and $a_{eff} \propto l_p$ is the effective radius of molecule. The simulations of monatomic liquids with different types of interaction potentials reveals that $a_{eff}(T) \equiv const$, and the E-S relation may be presented as: $\nu \cong l_p^2 T/(CMD)$, where $C \approx 8$ [4, 16]. The experimental examination of this relation for dusty plasma is presented in Table 1, where the measured values of C are shown. We can see that for all cases under study the C values are close to 8 within 5-10%.

Here we also present the comparison of the measured transport constants with the data of simulation of the 2d-, and 3d- systems with a screened potential. The Γ^* and ξ values can be estimated from the measurements of $D(t)$ functions [17, 22]. Numerical simulations have shown that the behavior of $D(t)$- function in the liquid systems for the time less than some critical value ($t < 2/\omega^*$) is similar to the $D(t)$ for particles in solid. This function may be obtained from the motion equation of a harmonic oscillator with some characteristic frequency ω_c [16,17]

$$\frac{D(t)}{D_o} = \frac{1-\exp(-\nu_{fr} t/2)\left(ch(\nu_{fr} t\psi) + sh(\nu_{fr} t\psi)/\{2\psi\}\right)}{2\xi_c^{\,2}\nu_{fr} t}, \qquad (3)$$

where $\psi = \frac{\sqrt{1-8\xi_c^{\,2}}}{2}$, and $\xi_c = \frac{\omega_c}{\nu_{fr}}$. In the case of 3-d systems ($\kappa<6$), the value of ω_c is equal to the characteristic frequency of particles in *bcc*-type lattice: $\omega_{bcc}^2 = (2eZ)^2\exp(-\kappa)(1+\kappa+\kappa^2/2)/(l_p^3 M\,\pi)$ [17]. In the case of 2d-hexagonal crystal, the frequency ω_c is determined from $\omega_c^2 = \omega_h^2 \approx 1.35\,\omega_{bcc}^2$ [16]. These results are in agreement with the measurements of $D(t)$- function for dusty plasma in gas discharges [17, 22]. Procedure of best fitting of experimental $D(t)$- functions by the Eq. (3) is illustrated in Fig. 4.

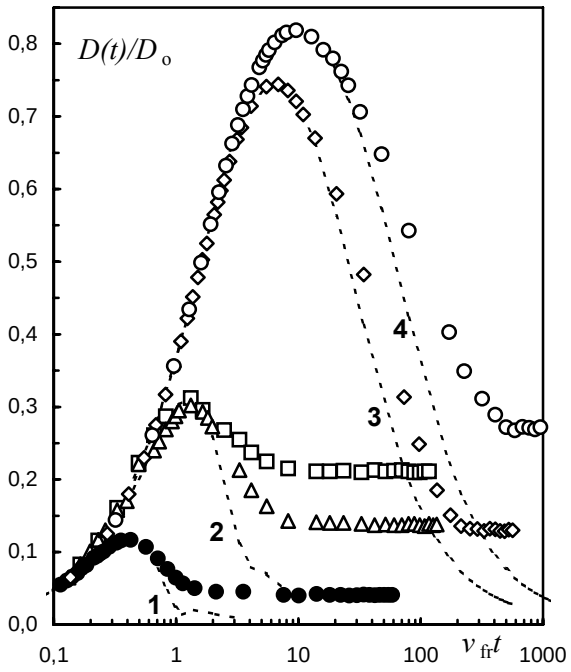

FIGURE 4. Experimental $D(t)/D_o$ functions for different experiments: (●) – a_p = 6.73 μm, P = 11 Pa, W_d =2 mW; (△) – a_p = 6.73 μm, P = 19 Pa, W_d =5 mW; (□) – a_p = 6.73 μm, P = 19 Pa, W_d =15 mW; (◇) – a_p = 0.95 μm; P = 15 Pa, W_d =7 mW; (○) – a_p = 1.7 μm; P = 67 Pa, W_d =20 mW. And illustration of best fitting of $D(t)/D_o$ by the Eq. (3) with ξ_c : **1** - 3.8; **2** - 1.2; **3** - 0.18; **4** - 0.1.

With knowing the dust temperature, one can retrieve ξ_c and D_o from these measurements, that, in turn, allows to determine both the Γ^* and $\xi = \omega^*/\nu_{fr}$ values in case of 2d- ($\omega_c=\omega_h$), or 3d- ($\omega_c=\omega_{bcc}$) systems. In our experiments, we can consider two estimations for the Γ^* and ξ values for both limiting cases (see Table 1).

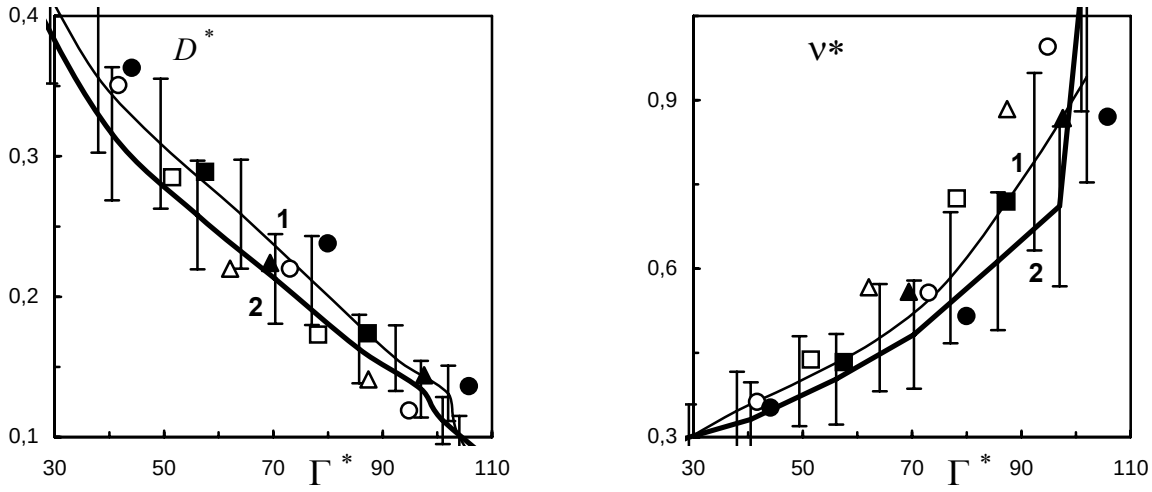

(a) **(b)**

FIGURE 5. Normalized diffusion D^*(**a**), and viscosity ν^* (**b**) coefficients vs. Γ^* retrieved under assumptions $\omega_c = \omega_h$ (●;▲;■) and $\omega_c = \omega_{bcc}$ (○;△;□) for different experiments: (●;○)– a_p = 6.73 μm; (▲;△)– a_p = 0.95 μm; (■;□)– a_p = 1.7 μm. Hard lines are the results of numerical simulations for **1** – 3d- systems; **2** – 2d- systems.

The comparison of the measured transport constants with the numerical data [10, 16] are shown in Fig. 5, where the normalized diffusion, $D^*=D(1+\xi)/D_o$, and viscosity $\nu^* = \nu/\{\nu_{fr} l_p^2 (1+\xi)\}$ coefficients are presented.

To conclude, results the examination of the E-S formula has shown, that the relation between the viscosity, ν, and diffusion constants, D, for particles in strongly coupled dusty plasma can be approximated by the expression: $\nu \approx l_p^2 T/(8MD)$, for the wide range of dusty plasma parameters.

3.2. Experimental Study of the Heat Transport Processes in Dusty Plasma Fluid

In the case of heat transfer (no convection), the heat flux density $\boldsymbol{q}$ obeys the Fourier law

$$q = - \chi \nabla T / k_B, \tag{4}$$

where $\boldsymbol{q} = 0.5[\int \boldsymbol{V} M V^2 dN]/S\delta x$ is the heat flux transferred by particles at velocity $\boldsymbol{V}$ through an area S of a layer of matter of thickness δx, and N is the number of particles. In the absence of vibrations and rotation of particles and assuming their energy to be uniformly distributed over the degrees of freedom, the density of heat flux propagating in the preferred direction **x** may be found as $q \approx 1.5\rho(\langle V_x^3\rangle_+ - \langle V_x^3\rangle_-)$, where $1.5\rho\langle V_x^3\rangle_{+(-)}$ is the amount of heat transferred in the direction of (+) and counter to (-) the flow. Then, one can write for the coefficient χ

$$\chi \approx 1.5\, n\, \delta x\, k_B (\langle V_x^3\rangle_+ - \langle V_x^3\rangle_-) (\langle V_x^2\rangle_+ - \langle V_x^2\rangle_-)^{-1}. \tag{5}$$

(In this case the thermal diffusivity may be obtained, as $\theta = \chi/(\rho c_p) \cong 2\chi/(5n k_B)$.)

The nonuniform distribution of the dust temperature in plasma (including a highly nonisotropic distribution) is observed quite frequently [34–37]. This phenomenon may be explained by spatial variation of dust charges, which provides for the formation of internal heat sources, Q_h, in a system. Because Eqs. (4)–(5) are valid for an inhomogeneous medium as well; a possibility exists of obtaining the temperature dependence of heat-transfer coefficients.

Experiments in RF-discharge. The experiments on a study of heat transfer were performed in plasma of rf-discharge in argon ($P \approx 20$ Pa) with Al_2O_3 particles ($a_p \approx 2$ μm, $\rho_p \approx 2.4$ g cm^{-3}). The scheme of experiment is given in Fig. 6 a. The particles of a dust cloud were illuminated by a plane beam of *He-Ne* laser (with a laser sheet ~ 250 μm) for detailed study of dust structures and their dynamics. The analyzed monolayer was videofilmed using a CCD camera (frame frequency, 50 s^{-1}). Analyses were performed for 5-7 horizontal dust layers placed close to a center of dust cloud. The coordinates and trajectories of particles were obtained as a result of video records processing.

Under the experiments, the dust cloud was initially an equilibrium liquid structure consisting of ~13–15 dust layers ~3.5 cm in diameter. As a result of minor variation of the discharge parameters (power or pressure), one of the cloud edges was heated rapidly. Front of the propagation of thermal perturbation was flat; the perturbation propagated in the single (horisontal) direction **x** (see Fig. 6 b). We have registered no any temperature gradients in other directions. We have also observed no dust drifts or convections in analyzed structures for stationary cases as well as for unsteady-state heat transport. (Distributions of dust velocities were close to Maxwell's functions.)

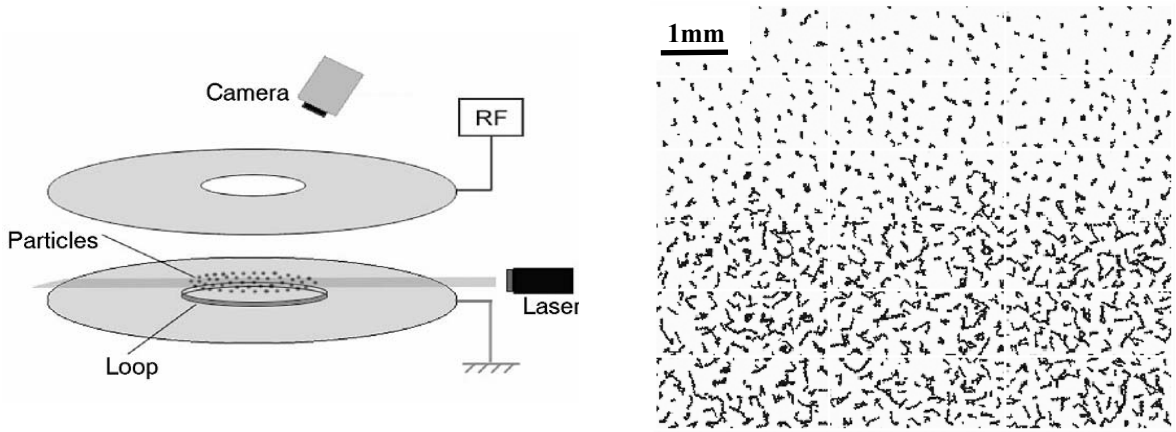

FIGURE 6. The scheme of the experiment (a) and video image of stable two-phase dust structure (b) with the trajectories of separate particles for time $t = 0.25$ s.

The thermal perturbation propagated through dust structure in the horizontal direction during ~12-13 s. Then the dust system aroused a new equilibrium state with a clearly defined interface between the low-temperature and high-temperature regions (see Fig. 6 b) and during another ~ 300 s the characteristics of observed dust structure were held practically constant. The parameters of the high-temperature region were as follows: $T \approx 3$ eV, $l_p \approx 400$ μm, $\Gamma^* \approx 6$, $\omega^* = (T\Gamma^*/(\pi M l_p^2)\}^{1/2} \approx 8.5$ s^{-1}. The low-temperature region exhibited characteristics close to the parameters of an unperturbed system: $T \approx 0.3$ eV, $l_p \approx 500$ μm, $\Gamma^* \approx 49$, $\omega^* \approx 6.8$ s^{-1}. The temperature was analyzed using the measurements of the dust velocity distributions; the mean distance l_p and parameter Γ^* were determined from the experimental pair correlation function (see Fig. 7). The errors in temperatures and Γ^*measured, were about 10%, the errors in determination of l_p was less than 5%. The friction coefficient was $\nu_{fr} \approx 35$ s^{-1} in a free-molecular approach [38].

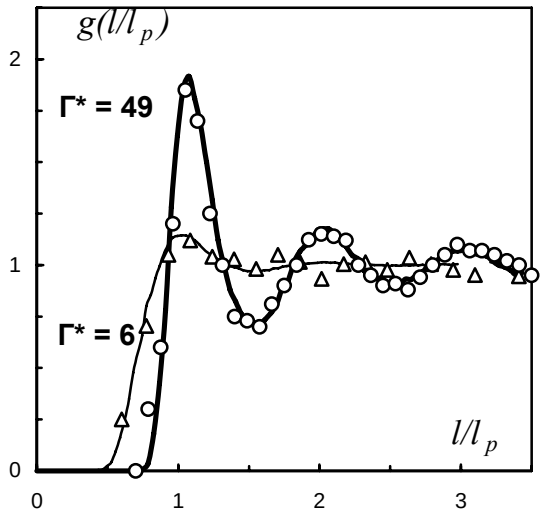

FIGURE 7. Experimental pair correlation functions $g(l/l_p)$ for: (△)- high-temperature, and (○) – low-temperature regions. Continuous lines are the results of numerical simulations for the appropriate Γ^* parameters.

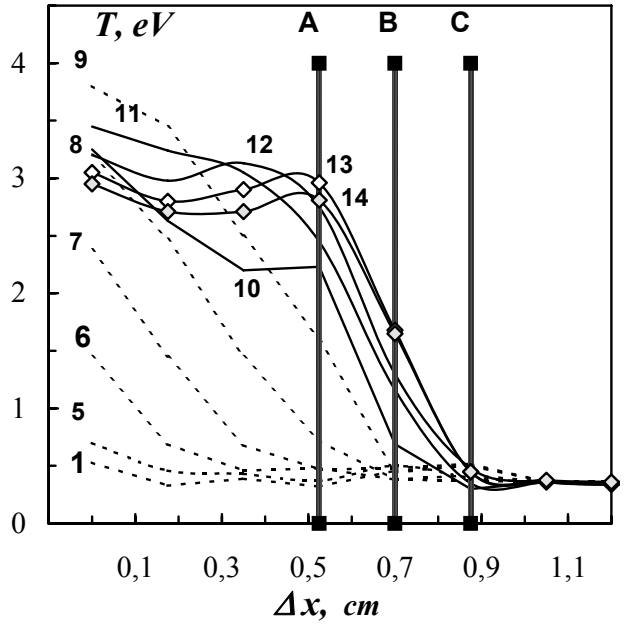

FIGURE 8. Spatial distribution of thermal perturbation for different times of observation. The numerals indicate the time in seconds; $\Delta x = m\ \delta x$, where m is number of analyzed regions of width δx. Vertical lines show the regions of measurement of χ in the steady state.

Because the analysis of measured dust velocity has not revealed any convective (or another regular) motion, we can suppose that both convections and diffusions are lacking in our experiments, and that the observed heat transport is associated with a thermal conduction in dusty component. The results of determining the conductivity χ using Eq. (5) for steady-state conditions (t > 13 s) on the interface for the A–C region of width ~ $2\delta x$ = 0.35 cm and, separately, for the A–B and B–C regions (see Fig. 8) are given in the Table 2 as functions of the average (for these regions) temperature. The errors in measured values of χ were about 10%.

Let us consider a dynamics of propagation of thermal perturbation assuming that this propagation is associated with a thermal conduction. For examination of this assumption we can estimate the time of equalization of temperature, $\tau_{eq} = L^2/(\pi^2\theta)$ using the values of the thermal diffusivity θ coefficients obtained in steady-state conditions $\theta \approx 0.01$ cm^2/s [39]. Then, for the characteristic length in the direction of heat propagation $L \approx 0.5$ cm we can derive $\tau_{eq} \approx 5$ c that is in agreement with the experimental observation.

TABLE 2. Coefficients θ and χ for steady state of a dust structure in rf-discharge

T, eV	Γ^*	$\chi\ 10^{14}$, erg/(s cm K)	θ, cm^2/s
2.7 [A;B]*	6.7	2.39	0.011
1.68 [A;C]	10.7	2.16	0.010
1.3 [B;C]	13	1.93	0.0089

* The location of analyzed region of dust structure (see Fig. 4) is shown in the brackets.

4. TRANSPORT PROPERTIES OF DUSTY PLASMA IN MICROGRAVITY

4.1. Diffusion of Macroparticles in Dusty Plasma Induced by Solar Radiation

Here, results of an experimental study of diffusion of dust particles, charged by photoemission under microgravity conditions are presented. Experiments were performed in 1997 at the Mir orbital complex by a group of scientists from the Institute of High Energy Densities together with the Energiya Rocket-Building Corporation. The data were obtained, which have shown that under the action of intensive solar radiation the micron-size particles can acquire considerable positive electric charges [30,31]. The experimental study of dust diffusion was performed for bronze particles with the mean radii $a_p \cong 37.5$ μm in background gas (neon) at the pressure $P \cong 40$ Tor. The particles were contained in a cylindrical glass tube, the bottom of which was the uviol window intended for the solar irradiating of dust cloud (Fig. 9). Extra irradiating of particles by a laser beam was used for improved diagnostics. Subsequently videorecords were handled by a special program for the identification of the displacements of separate particles.

The first step of experiments was the observation of dust particles without the action of solar radiation. During the observations (~20 min) the number of particles in the field of view of videosystem did not vary significantly. The second step was the observation of particles while irradiating the dust cloud with solar radiation. In an initial state, the bronze particles were on the walls of the tube. Therefore, the experiments were carried out as: (1) dynamic action on the system with the closed window; (2) exposure in darkness ~ 4 s $>> \nu_{fr}^{-1}$ to reduce of initial dust velocities; (3) irradiating of the tube by solar radiation; (4) relaxation of the particles to the initial state (the leaving to ampoule walls) for the time ~ 3-5 min. This interval is about three order of magnitude shorter than the time for full diffusion losses of particles at room temperature for their Brownian motion.

The initial dust concentration n_o was varied from 195 to 300 cm^{-3}. The dependencies the relative dust concentration $n(t)/n_o$ on the time t are shown in Fig. 10.

The photoemission charge of particles was obtained from the approximations of the curves $n(t)/n$ at $t > 40$ s by the method detailed in [30] and was close to $Z \approx 4\ 10^4$ (±15%). Velocities of the particles at the initial stage of irradiation were chaotic. Under the solar action, the dust motion acquired a directed motion forward the tube walls. For a time ~ 3 s after the beginning of solar irradiation, the dust stochastic kinetic energy is increased, and the interparticle correlation changed. The pair correlation functions are shown in Fig. 14. According to numerical calculations, the stabilization time for correlation in the dust cloud with $\omega_o/\nu_+ << 1$ ($\omega_o = Ze(n_o/M)^{1/2}$) is close to the time of thermalization of the system $\tau_{Maxw} \cong \nu_{fr}/4\pi\omega_o^2$, which in our case is ~ 4-6 s [30,40].

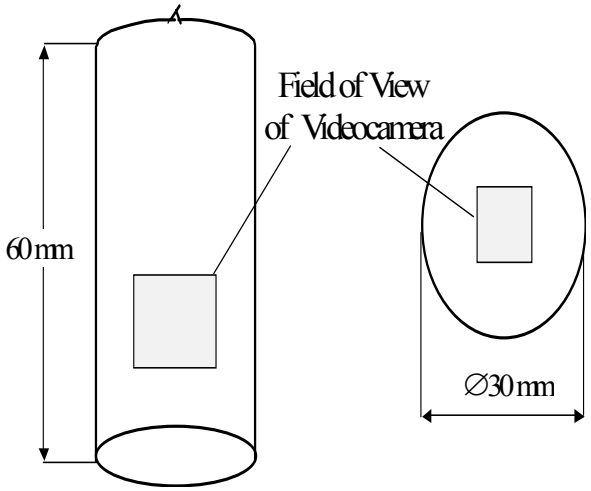

FIGURE 9. The geometry of the glass tube

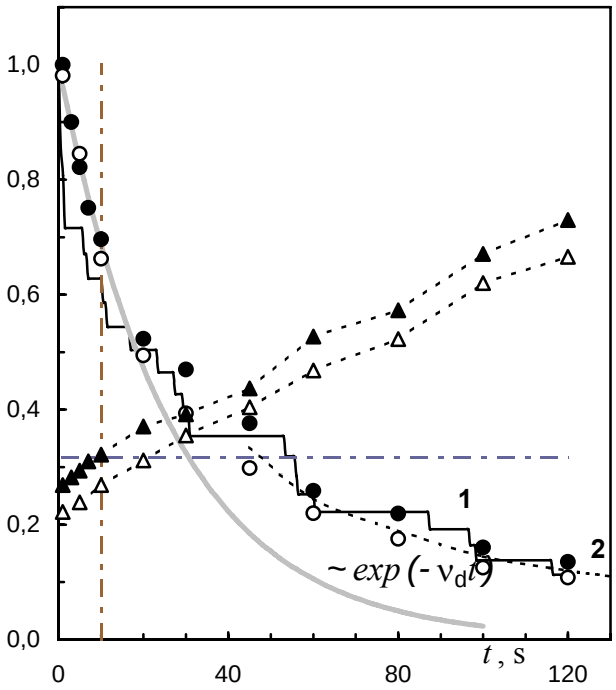

FIGURE 10. Dependencies of n/n_0 (●;○) and ratio of λ/R (▲;△)vs. time t for the different initial concentration n_o: (○;△)- 195 cm^{-3}; (●;▲)- 300 cm^{-3}. And the $n(t)/n_o$ function obtained by Brownian dynamic method (**1**) and its analytical approximation (**2**).

The dust temperature T was obtained from: $T_{x(y)} = m_+\{\langle V_{x(y)}^2\rangle - \langle V_{x(y)}\rangle^2\}$, where $\langle V_{x(y)}\rangle = V_d^{x(y)}$ is the regular drift velocity. Determining of the dust temperature for the various experiments gives $T_x \cong 51$ eV, $T_y \cong 22$ eV, within 5 %. The velocity distributions in the *OX*-, and *OY*-directions were close to Maxwellian. Similar non-uniform distributions of stochastic kinetic energy ($T_x \neq T_y$) and "abnormal heating" were observed in a various dusty plasma experiments and can be related to the temporally-spatial fluctuations of dust charge [34-37]. The temperature T_e^S of photoelectrons (which leave the particle's surface) depends on the material of the dust and, in most cases is ~ 1 - 2 eV, and under experimental conditions it is close to the electron temperature, T_e , in the dust cloud [30,31].

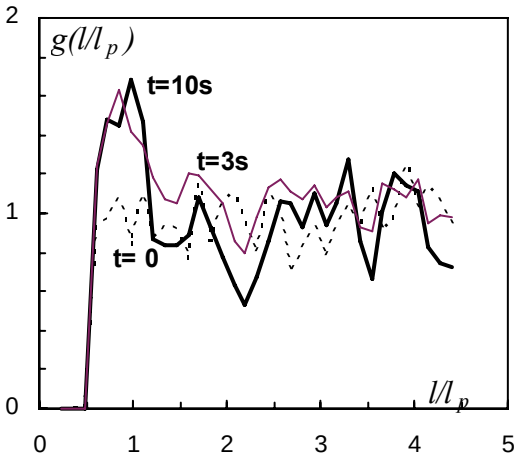

FIGURE 11. Pair correlation function $g(l/l_p)$ for different observation time t.

As the considered system consists of the positively charged macroparticles and the photoelectrons with the density $n_e \sim Zn$ emitted by them, it is possible to assume, that the transport properties of this system will depend on ambipolar diffusion of the particles. Because of the large difference of mobility of electrons μ_e and dust μ_+, a negative surface charge appears on the tube walls. The incipient polarization electric field blocks further partitioning of the charged components. Therefore, the electrons and the heavy dust particles can diffuse "together" with some effective coefficient D_a of ambipolar diffusion [38, 40]: $D_a = \{D_e \mu_+ + D_+ \mu_e\}/\{\mu_+ + \mu_e\}$, where $D_{e(+)} = T_{e(+)}/\nu_{e(+)} m_{e(+)}$ is the free diffusion constants for electrons (-) and particles (+), $T_{e(+)}$, $m_{e(+)}$ and $\nu_{e(+)}$ are the temperature, the mass and the frequency of collisions with the neutral gas molecules for electrons and dust, respectively ($\nu_+ = \nu_{fr}$, $T_+ = T$, $m_+ = M$). Then, in the case of $\mu_e >> \mu_+$, the ratio of diffusion constants can be represented in the form: $D_a / D_+ \approx 1 + Z T_e / T_+$. With the measured temperatures (T_x, T_y), the ratios of diffusion constants can be estimated as $D_a / D_+^x \approx 0.8\text{-}1.6\ 10^3$, and $D_a / D_+^x \approx 1.8\text{-}3.6\ 10^3$ for $T_e = 1\text{-}2$ eV.

These estimations of D_a / D_+ ratio are valid only when the dissipation is determined by collisions with gas neutrals, and the collisions of charged components are negligible. On the other hand, ambipolar diffusion is determined by the polarization effects, which are impossible in a dilute plasma with a low density of charged components. In a plasma with the density n, the diffusion have a ambipolar character when $\delta n = |n_e - n_+| << n \approx n_e \approx n_+$. For cylinder with the radius R, it is valid for $\delta n/n \approx (\lambda/R)^2 << 1$, where $\lambda^2 = T_e / 4\pi e^2 n_e$ [40]. Taking into account that $n_e \approx Zn_p$ we have $\delta n/n \approx 2.1\text{-}6.4\ 10^{-2}$ for the initial conditions $n = n_o$ under the assumption of $T_e \cong 1\text{-}2$ eV. The dependencies of λ/R on time are shown in Fig. 10 for $T_e = 2$ eV.

Assuming that for $\delta n/n < 0.1$ the losses of charges in our experiments are connected with their ambipolar diffusion to the ampoule walls, the area of ambipolar diffusion can be determined from the mean velocity of diffusion losses of macroparticles: $dn/dt = - n \nu_d$, where $\nu_d = D_a / \Lambda^2$ is the frequency of diffusion losses, and $\Lambda \approx R/2$ is some diffusion length [40]. The value of ν_d can be obtained from the experimental curve $n(t)/n_o$ at $t < 10$ s, where the $n(t)/n_o$ function agrees well with the solution $n = n_o \exp(-\nu_d t)$ for $\nu_d \approx 0.035$ s^{-1} (Fig. 10). Then, an estimate of ambipolar diffusion gives $D_a \approx 2\ 10^{-2}$ cm^2/s.

The free diffusion constants $D_+^{x(y)}$ were retrieved from the measurements of dust temperature, and drift velocity $V_d^{x(y)}$: $D_+^{x(y)}(t) = \{\langle \Delta l(t)^2 \rangle - (V_d^{x(y)} t)^2\}/2t$, where $\langle \Delta l(t)^2 \rangle$ is the mean-square displacement of separate particles in the direction of axis OX (or OY) as $D_+^x \approx 1.3\ 10^{-5}$ cm^2/s and $D_+^y \approx 5.7\ 10^{-6}$ cm^2/s. The value of ratio $D_+^x / D_+^y \approx 2.28$ agrees very well with the measured dust temperature, and both the measured ratios $D_a / D_+^x \approx 1538$, and $D_a / D_+^x \approx 3509$ are in agreement with the theoretical prediction.

To summarize, the complex experimental study of dynamics of macroparticles in dusty plasma induced by solar radiation were carried out. The investigated dust system represented a fluid ($\Gamma \sim 30$). The comparison of experimental data and theoretical estimates has shown that the dynamic behavior of macroparticles for $t < 10\text{-}15$ s can determined by ambipolar diffusion. Finally notice, that similar observations of ambipolar diffusion for charged macroparticles are not feasible under ground-based laboratory conditions.

4.2. The Dynamics of Macroparticles in a Direct Current Glow

Here, we describe the experiments performed aboard the Mir space station in 1998 during the 28th orbital expedition for large size bronze particles (fraction of 70–180 μm, mean radius $a_p = 62.5$ μm, $\rho_p = 8.2$ g/cm^3) in dc-discharge in neon (*Ne*) at pressure $P = 1$ Tor [20]. The simplified scheme of experimental setup is shown in Fig. 12. For diagnostics of macroparticles, a plane laser beam (~ 300 μm wide) was used. The image was recorded on a video tape at a 50 s^{-1} frame frequency. The data were processed using a special program.

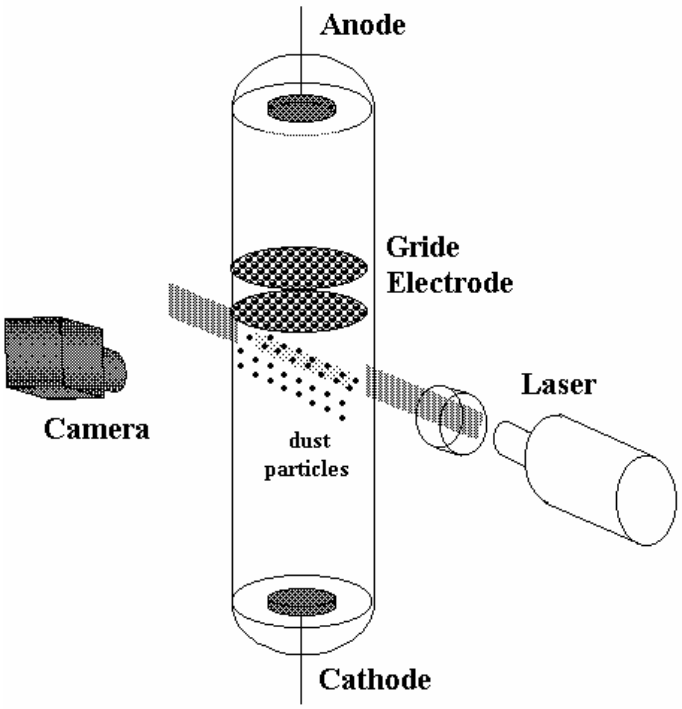

FIGURE 12. Schema of the experimental setup.

Experiments were performed at discharge currents I= 0.1–0.8 mA varied by the current source. Under experimental conditions, the discharge occurred in an anomalous mode, and the plasma concentration was $n_o \approx$ (5–14) 10^7 cm^{-3}. Here $n_o \approx n_e^o \approx n_i^o$, and $n_{e(i)}^o$ is the concentration of electrons (ions) without dust. Bronze particles were initially situated on tube walls. For this reason, the system was subjected to a dynamic action (pushed) after switching on a discharge to shake off particles from tube walls. After the dynamic action, bronze particles moved toward insulated grid electrodes, in the vicinity of which ordered structures were formed. The dimensions of dust clouds were about 2 cm in the radial direction and ~ 0.7–1.3 cm from the grid edge along the tube axis. Pair correlation functions $g(l)$ for various currents I are shown in Fig. 13. The mean interparticle distance l_p was changed from ~ 750 μm to ~ 1000 μm. The discharge was then "quenched," the particles relaxed to the initial state (went away to tube walls), and the experiment was repeated at a new discharge current value. The mean drift velocity V_p of particles from the positive column to the grid electrode was constant in the measurement volume. Because of this the dust charges $Z \approx 10^6$ were found from the equation: $v_{fr}V_p = E\,eZ/M$, where E is the value of electric field [20]. The Z values are practically independent of discharge current and correspond to the high surface potentials $\varphi_s = eZ/a_p \approx$ 35-37 V.

According to the Lindemann criterion, a solid phase melts if the ratio between the root of the mean-square displacement Δ_o of particles from their equilibrium positions and the mean interparticle distance l_p reaches about 0.15 [41]. In experiments, particle displacements are usually measured from the center of mass of the system, that is, $\Delta = \sqrt{2}\Delta_o$, and the Lindemann parameter at the melting curve is therefore $\delta_c = \Delta/l_p \approx 0.21$. The $\delta_c(t) = \Delta_N(t)/l_p$ time dependence here, $\Delta_N(t)=\sqrt{\left\langle (\mathbf{l}(t)-\mathbf{l}(0))^2 \right\rangle_N}$, $\mathbf{l}(t)$- is the displacement of a separate particle, and $\langle\ \rangle_N$ denotes averaging over the ensemble of N particles] for 16 particles (N_p = 16) is shown in Fig. 14. Note that, during some time intervals, the $\Delta_N(t)/l_p$ ratio remains constant and corresponds to the Lindemann criterion.

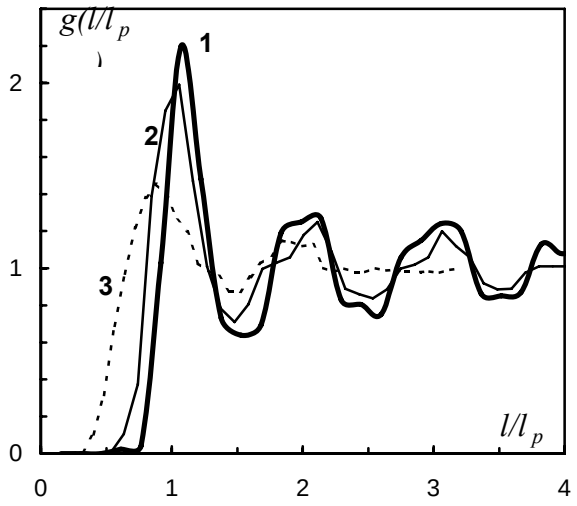

FIGURE 13. Pair correlation functions $g(l/l_p)$ for dust structures formed close to grid electrodes at discharge currents I of (***1***) 0.1, (***2***) 0.4, and (***3***) 0.8 mA.

When the observation time was decreased to about 1 s, the number of identified trajectories increased to N_p = 70–120 at the expense of particles that experienced transitions between "settled" states from one cloud region to another. Averaging of particle displacements Δ_N(t)over the ensemble was then close to time averaging, $\Delta_N^t = \sqrt{\left\langle \left\langle \mathbf{l}(t) - \mathbf{l}(0) \right\rangle_N \right\rangle_t^2}$. Here, $\langle\ \rangle_{N,\,t}$ denotes averaging over the ensemble and time. A similar picture was observed in simulations of the particle dynamics for a strongly nonideal liquids [10] close to the crystallization point.

The dust diffusion coefficients, $D \sim$ 0.1-1.1 mm^2/s, were found from the measured mean-square displacements. The measured D values were increased with the discharge current I. The dust temperature $T \sim 10^5$ eV was obtained by the best fitting of dust velocities spectrum by the Maxwell distribution. The mean chaotic (thermal) velocities of

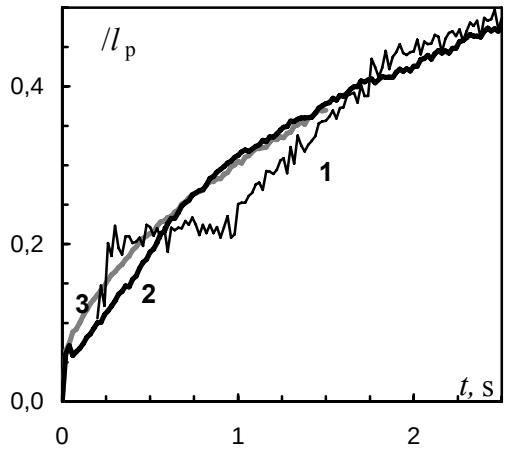

FIGURE 14. Experimental value of Lindemann parameter $\delta_c = \Delta(t)/l_p$ (I = 0.4 mA) obtained as: **1** -$\Delta(t) \equiv \Delta_N$(t), N_p=16; **2**- $\Delta(t) \equiv \Delta_N^t$ (t), N_p=16, ; **3**- $\Delta(t) \equiv \Delta_N^t$ (t), N_p=96.

dust were ~1 mm/s. The determination of effective coupling parameter, Γ^*, was performed from the measurements of the mean interparticle distance l_p, temperature T, and the D diffusion coefficient using the relation [10]

$$D_p \cong \frac{T_p \Gamma^*}{12\pi(\omega_l + \nu_{fr})m_p} \exp\left(-3\frac{\Gamma^*}{\Gamma_c}\right), \quad (6)$$

where $\Gamma_c \approx 102$, and $\omega_l \equiv (\Gamma^* T_p/\pi\, l_p^2\, m_p)^{1/2}$. The Γ^* parameters reproduced from (6) are shown in Fig. 15 for the mean, and minimal sizes of particles. Note that the friction coefficient ν_{fr} does not significantly influence on the Γ^* value ($\nu_{fr} < \omega_l$ under study). An analysis of Γ^* under the assumption of negligibly weak screening ($\Gamma^* = \Gamma$, $\kappa < 1$) gives a minimal estimation of the dust charge Z, and it allows the determination of dust surface potentials. This gives $\varphi_s \approx 42$ V for medium-sized particles $a_p = 62.5$ μm and $\varphi_s \approx 30$ V for particles with $a_{min} = 35$ μm at $I \le 0.5$ mA. For $I = 0.8$ mA, the recorded surface potential value is lower by approximately 30%. The obtained charges are in agreement with the results of determining Z from the equation of motion.

Thus, we can hope that the obtained φ_s correctly reproduces real dust charge, and, accordingly, the assumption of weak screening ($\kappa < 1$) of dust well corresponds with the experimental conditions under study.

Note that high dust charges $Z \approx 10^6$ at their concentrations $n \approx 10^3$ cm^{-3} do not correspond with the suggestion of the electroneutrality in the system, $Zn + n_e = n_i$, if we assume that the presence of dust have no significant influence on discharge conditions and the concentration of ions in the dust cloud is comparable with their concentration in the absence of macroparticles, $n_i^o \approx 10^8$ cm^{-3}. Such a discrepancy has already been observed in laboratory conditions on the Earth [42], where the authors suggested that the abnormally high dust charges Z may cause by a change in the discharge conditions in the dust cloud.

To summarize, the results of experimental studies of the dynamics of macroparticles in a dc- discharge in microgravity were presented. The measurements showed that the observed dust structures were a dust liquid, and their dynamics was in close agreement with the simulation of systems with weak screening ($\kappa < 1$). Experimental estimates of dust charges corresponded to surface potentials ~ 30– 40 V, which far exceeded values predicted by the OML theory. This discrepancy could be related to both a decrease in the effective flow of ions onto particles whose radii were larger than the free path of ions and an increase in the electron temperature in the dust cloud because of an influence of dust on equilibrium ionization in dc- discharge [20]. Note, that experiments on studying interaction potentials and charging processes for large size hundred-micron particles in a dusty plasma cannot be performed under ground-based conditions.

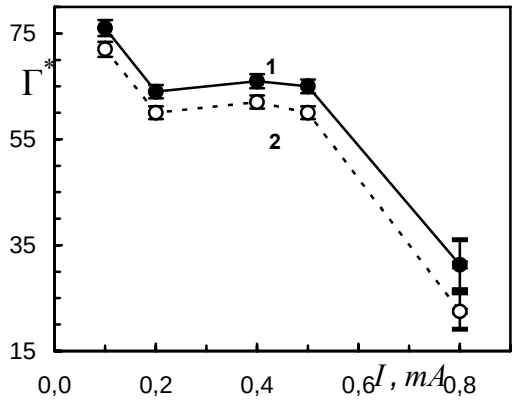

FIGURE 15. Parameters Γ^* reproduced from diffusion measurements for particles of different sizes:**1** - $a_p = 62.5$ μm; **2** - $a_{min} = 35$ μm; error intervals are shown.

5. CONCLUSION

Results of a complex experimental study of the transport properties of dusty plasmas are presented. The experiments were performed for a wide range of dusty plasma parameters under the ground-based, and microgravity conditions.

Experimental study of the kinematic viscosity and the diffusion are presented for macroparticles in dusty plasma under the ground-based conditions. The experiments are performed in plasma of a capacitive rf- discharge with the particles of different sizes (~ 0.95; 1.7 and 6.73 μm). Experimental examination of the Einstein-Stokes relation between the viscosity and diffusion constants is carried out. The results are given of an experimental investigation of heat transport processes in fluid dusty structures in rf-discharge plasmas under different ground-based conditions: for discharge in argon, and for discharge in air under an action of electron beam. The analysis of steady-state and unsteady-state heat transfer is used to obtain the coefficients of thermal conductivity and thermal diffusivity. The temperature dependence of these coefficients is obtained. The results of a comparison of the measured transport constants with the existing data of numerical simulation are considered.

Diffusion of bronze macroparticles, charged by the solar radiation in microgravity are studied by analyzing of experimental data obtained on the MIR space station. The comparison of experimental and theoretical estimates has shown that the dynamic behavior of macroparticles for the small observation time can determined by ambipolar diffusion. The dynamics of large-sized (70–180μm) spherical bronze particles in a direct current glow discharge plasma was studied experimentally under microgravitation conditions at the Mir orbital complex. The temperatures, velocities, pair correlation functions, and self-diffusion coefficients of macroparticles were measured at various discharge currents. The charges of dust particles (on the order of $10^6 e$) corresponded to high surface potentials of about 30–40 V.

6. ACKNOWLEDGMENTS

This work was supported by Complex Research Program of the Presidium of Russian Academy of Sciences "Study of Matter under High Energy Densities", by Max Planck Award Cooperation Research Program "Physics of High Energy Density Plasmas", by the Russian Foundation for Basic Research (Grants No.06-02-17532, No. 06-02-81052 and No. 06-02-01569), by NWO (Project 047.016.020) and by the Russian Science Support Foundation.

7. REFERENCES

1. *Photon Correlation and Light Beating Spectroscopy*, H.Z. Cummins and E.R. Pike, Eds., Plenum, New York (1974).
2. Ya.I. Frenkel', *Kinetic Theory of Liquids*, Clarendon Press, Oxford, 1946.
3. H.J. Parkhust, Jr., and J. Jonas, J. Chem. Phys. **63**, 2705 (1975).
4. N. H. March and M.P. Tosi, *Introduction to liquid state physics,* World Scientific, 1995.
5. B. Pullman, *Intermolecular Interactions: From Diatomics to Biopolymers*, Wiley Interscience, Chichester, 1975.
6. H. Lowen, J. Phys.: Condens. Matter **4**, 10105, (1992)
7. V. Nosenko and J. Goree, Phys. Rev. Lett. **93**, 155004 (2004).
8. A. Gavrikov, I. Shakhova, A. Ivanov, *et al.*, Physics Letters A **336**, 378-383, (2005)
9. B. Alder, T. Wainwright, Phys. Rev. A, **1**, 18 (1970).
10. O.S. Vaulina and S.V. Vladimirov, Phys. Plasmas **9**, 835 (2002).
11. H. Ohta and S. Hamaguchi, Phys. Plasmas **7**, 4506 (2000).
12. T. Saigo and S. Hamaguchi, Phys. Plasmas **9**, 1210 (2002).
13. J. Wallenborn and M. Baus, Phys. Rev. A **18**, 1737 (1978).
14. Z. Donko, J. Goree, P. Hartmann, and K. Kutasi, Phys. Rev. Lett. **96**, 145003, (2006)
15. B. Liu and J. Goree, Phys. Rev. Lett. **94**, 185002, (2005)
16. O. S. Vaulina, I.E. Drangevski, Physica Scripta T**73**, 577-586 (2006)
17. O. S. Vaulina, O. F. Petrov, V. E. Fortov, JETP **99**, 711–721 (2005)
18. B. Liu, J. Goree, O. S. Vaulina, Phys. Rev. Lett. **96**, 015005 (2006)
19. V. E. Fortov, O. S. Vaulina, O. F. Petrov, *et al.,* Phys. Rev. Lett. **90**, 245005 (2003).
20. A.P. Nefedov, O.S. Vaulina, O.F. Petrov, *et al.*, JETP **95**, 673 (2002).

21. V.E. Fortov, O.S. Vaulina, O.F. Petrov, *et al.*, JETP **96**, 704 (2003).
22. O.S. Vaulina, O.F. Petrov, V.E. Fortov, *et al.*, Plasma Physics Reports **29**, 606 (2003).
23. O. S. Vaulina, O. F. Petrov, V. E. Fortov, *et al.*, Phys. Rev. Lett. **93** (3), 035004 (2004).
24. S. Nunomura, D Samsonov, S. Zhdanov *et al.*, Phys. Rev. Lett. **96**, 015003 (2006).
25. S. Ratynskaia, K. Rypdal, C. Knapek *et al.*, Phys. Rev. Lett. **96**, 105010 (2006).
26. C.H. Chiang and Lin.I. *et al.*, Phys. Rev. Lett. **77**, 647 (1996).
27. G.E. Morfill, V.N. Tsytovich, and H. Thomas, Plasma Phys. Rep. **29**, 1 (2003).
28. V.E. Fortov, A.G. Khrapak, S.A. Khrapak, *et al*., Physics- Uspekhi **174**, 495 (2004); M.H. Thoma, M. Kretshmer, H. Rothermel, *et al*., American Journal of Physics **73**, 420 (2005).
29. S.V. Vladimirov and M. Nambu, Phys. Rev. E **52**, R2172 (1995).
30. V. E. Fortov, A. P. Nefedov, O. S. Vaulina, *et al.,* JETP 87, 1087 (1998).
31. O. S. Vaulina, A. P. Nefedov, O. F. Petrov, *et al.,* Phys. Rev. Lett. 88, 035 001 (2002)
32. V. E. Fortov, A. P. Nefedov, V. I. Molotkov, *et al.,* Phys. Rev. Lett. 87, 205 002 (2001).
33. G. Morfill, H. Thomas, U. Konopka, *et al.,* Phys. Rev. Lett. 83, 1598 (1999).
34. O.S. Vaulina, A.A. Samarian, O.F. Petrov et al, *Plasma Phys. Rep.* **30**, 652 (2004).
35. V.I. Molotkov, A.P. Nefedov, V.M. Torchinskii, *et al.*, JETP **89**, 477 (1999).
36. V.V. Zhakhovskii, V.I. Molotkov, A.P. Nefedov *et al., JETP Lett.* **66**, 419 (1997).
37. O.S.Vaulina, S.A. Khrapak, O.F.Petrov, *et al*. Phys. Rev. **60**, 5959б (1999).
38. E.M. Lifshitz, L.P. Pitaevskii, *Physical kinetics* (Pergamon Press, Oxford New York, 1981).
39. L.D. Landau, E.M. Lifshitz, *Fluid Mechanics*, (Pergamon Press, Oxford New York 1987).
40. Y.P. Raizer, *The Physics of Gas Discharge* (Berlin: Springer Verlag, 1991).
41. F. A. Lindemann, Z. Phys. **11**, 609 (1910).
42. A. M. Lipaev, V. I. Molotkov, A. P. Nefedov, *et al.*, JETP **85**, 1110(1997).